water

MDPI

Article

Uptake of Sb(V) by Nano Fe_3O_4-Decorated Iron Oxy-Hydroxides

Konstantinos Simeonidis [1,2,*], Kyriaki Kalaitzidou [1], Efthimia Kaprara [1], Georgia Mitraka [1], Theopoula Asimakidou [3], Lluis Balcells [4] and Manassis Mitrakas [1]

1 Analytical Chemistry Laboratory, Department of Chemical Engineering, Aristotle University of Thessaloniki, 54124 Thessaloniki, Greece; kikikal83@hotmail.com (K.K.); kaprara@auth.gr (E.K.); christinamitraka@gmail.com (G.M.); manasis@eng.auth.gr (M.M.)
2 EcoResources P.C., 55131 Kalamaria, Thessaloniki, Greece
3 Department of Physics, Aristotle University of Thessaloniki, 54124 Thessaloniki, Greece; tasimaki@physics.auth.gr
4 Institut de Ciència de Materials de Barcelona, Campus Universitat Autònoma de Barcelona, 08193 Bellaterra, Spain; balcells@icmab.es
* Correspondence: ksime@physics.auth.gr; Tel.: +30-231-099-8032

Received: 15 December 2018; Accepted: 15 January 2019; Published: 21 January 2019

Abstract: The presence of antimony in water remains a major problem for drinking water technology, defined by the difficulty of available adsorbents to comply with the very low regulation limit of 5 μg/L for the dominant Sb(V) form. This study attempts to develop a new class of water adsorbents based on the combination of amorphous iron oxy-hydroxide with Fe_3O_4 nanoparticles and optimized to the sufficient uptake of Sb(V). Such a Fe_3O_4/FeOOH nanocomposite is synthesized by a two-step aqueous precipitation route from iron salts under different oxidizing and acidity conditions. A series of materials with various contents of Fe_3O_4 nanoparticles in the range 0–100 wt % were prepared and tested for their composition, and structural and morphological features. In order to evaluate the performance of prepared adsorbents, the corresponding adsorption isotherms, in the low concentration range for both Sb(III) and Sb(V), were obtained using natural-like water. The presence of a reducing agent such as Fe_3O_4 results in the improvement of Sb(V) uptake capacity, which is found around 0.5 mg/g at a residual concentration of 5 μg/L. The intermediate reduction of Sb(V) to Sb(III) followed by Sb(III) adsorption onto FeOOH is the possible mechanism that explains experimental findings.

Keywords: drinking water; antimony; Fe_3O_4 nanoparticles; iron oxy-hydroxide; adsorbent; isotherms; SEM; XRD

1. Introduction

The occurrence of antimony in groundwater is generally attributed to natural release mechanisms and anthropogenic activities [1]. Suggestively, antimony-polluted water resources are usually located in areas affected by natural geochemical processes or acid mine drainage able to trigger the oxidative dissolution of sulfide minerals [2]. The extensive use of antimony trioxide as a flame retardant can be another possible source of pollution. In spite of the low frequency of antimony concentrations above 0.2 μg/L in water supplied for drinking purposes, the very low regulation limit set by authorities (5 μg/L in EU) signifies its high toxicity. Particularly, long-term consumption of water polluted with antimony is probably related to cancer development and other diseases [3]. Similarly to arsenic, the oxidation state of aqueous antimony species may be +3 or +5 according to the aerobic conditions in the groundwater reservoir. However, the coordination in oxy-anionic forms and the corresponding speciation are much more different to those of arsenic [4]. For Sb(V), which is the

commonly met oxidation state, $Sb(OH)_6^-$ is the dominant species in the pH range of natural water. The octahedral geometry of $Sb(OH)_6^-$ actually defines the sorption behavior of Sb(V) on metal oxy-hydroxides, since the larger dimensions inhibit successful approach and chemisorption on the surface. Thus, pentavalent species appear with higher mobility and meet stronger competition by other anions such as phosphates, silicates and bicarbonates [5]. On the other side, although Sb(III) is coordinated in a neutrally charged form, $Sb(OH)_3$, its adsorption is much more favorable by typical metal hydroxide adsorbents. Nevertheless, Sb(III) species are very susceptible in oxidation to Sb(V), while they are considered much more toxic to humans.

The removal of antimony species at residual concentrations below 5 μg/L is not always an easy task. A large-scale process such as coagulation/filtration using ferric or aluminum salts is able to capture both Sb(III) and Sb(V) [6,7], being also very efficient for the uptake of arsenic, which very frequently co-exists with antimony in polluted water resources [8]. However, coagulation/filtration has important drawbacks related to the large dimensions of the facilities and the large volumes of wastes that need to be handled. An alternative, oriented to application in point-of-use systems, is reverse osmosis which is, unfortunately, a nonselective and high-cost technique. Therefore, the development of selective adsorbents for antimony would be very advantageous considering the simplicity and automation induced by such a process [9]. Until now, several materials have been tested as antimony adsorbents including zero-valent iron [10], graphene oxide [11], activated alumina [12] and zeolites [13]. The best results were obtained for iron oxy-hydroxides with an adsorption capacity of 3 mg/g succeeded for Sb(III) at the regulation limit [14]. The potential of hematite-modified magnetic nanoparticles to capture Sb(III) below 5 μg/L has been also supported [15]. However, the efficiency of these adsorbents is limited only to the Sb(III) species, with a complete failure observed against Sb(V), which is the dominant form in most groundwater sources [16]. Suggestively, hydrated ferric oxides supported by calcite sand and zero-valent-iron-decorated functionalized carbon nanotubes were able to reduce Sb(V) concentration to parts-per-billion levels, but only for large solid-to-pollutant ratios [17,18]. Furthermore, even the capture of the Sb(III) is not always a nonreversible effect, since a possible oxidative environment may catalyze Sb(V) generation and re-dissolution of the latter [19,20]. Apart from the mentioned interfering water constituents, the presence of arsenic may provide an extra negative effect to the removal of Sb(V) by iron oxy-hydroxides [8], as also found during the operation of the Melivoia water plant in Thessaly, Greece [21].

The motivation of this work was the development of an adsorbent specified in the sufficient uptake of Sb(V) in compliance with the drinking water regulations and the requirements for long-term chemical stability and low-cost preparation. The novelty of such a product, which aims to cover the complete absence of antimonite-specified adsorbents, is based on the combination of two active inorganic phases. Particularly, a composite system consisting of an amorphous iron oxy-hydroxide (FeOOH) decorated with Fe_3O_4 nanoparticles was produced by sequential aqueous precipitation of iron salts and evaluated for its potential to operate both as a reducing agent for Sb(V) and adsorbent for the resulting Sb(III) species. The following experimental study supports the validity of the assumed mechanism suggesting that the electron donation by Fe_3O_4 enables a significant increase of FeOOH adsorption efficiency against Sb(V). Results also demonstrate the potential of similar approaches based on synergy-phase adsorbents to provide sophisticated solutions in water treatment.

2. Materials and Methods

2.1. Synthesis

The studied Fe_3O_4/FeOOH nanocomposites were synthesized in a batch reactor by the sequential precipitation of iron salts under different acidity and oxidative conditions (Figure 1). Particularly, in the first step, the iron oxy-hydroxide was prepared by the precipitation of $FeSO_4$ at pH 6 and a redox of 300 mV controlled by the addition of NaOH and H_2O_2 solutions, respectively. A quantity of 6.5 g of $FeSO_4 \cdot 7H_2O$ was added in a 600 mL glass beaker and dissolved in 400 mL of distilled water under

mechanical stirring. Then, a proper volume of 5 wt % NaOH solution was rapidly added to increase the pH up to 6, while another volume of 5 wt % H_2O_2 was introduced to establish the required redox potential. Immediately, the formation of a brown precipitate was observed. The reaction mixture was kept under slow stirring for one hour to allow ageing of the product and then the solid was washed several times with distilled water to eliminate reaction byproducts and oxidative residuals. A neutralized dispersion of 2 g FeOOH on dry basis was received at a volume of 200 mL and placed in a second beaker to serve as a seed for the precipitation of Fe_3O_4 nanoparticles by $FeSO_4$ and $Fe_2(SO_4)_3$. In the second step, a solution prepared by the dissolution of 2.4 g of $FeSO_4 \cdot 7H_2O$ and 3.6 g of $Fe_2(SO_4)_3 \cdot xH_2O$ (20 wt % Fe basis) into 200 mL of distilled water was mixed with the FeOOH dispersion. Such proportions correspond to the synthesis of the nanocomposite with a 50 wt % content in Fe_3O_4. Then, a quantity of 5 wt % NaOH solution was added to achieve a pH value 12 and allow the formation of a black precipitate consisting of Fe_3O_4 nanoparticles. After another hour of ageing, the final product was washed with distilled water, centrifuged and dried at room temperature. To modify the Fe_3O_4 content of the final product, the quantities of $FeSO_4$ and $Fe_2(SO_4)_3$ were varied proportionally. The Fe_3O_4/FeOOH nanocomposite was used in adsorption experiments in the form of ground powder sieved below 63 μm.

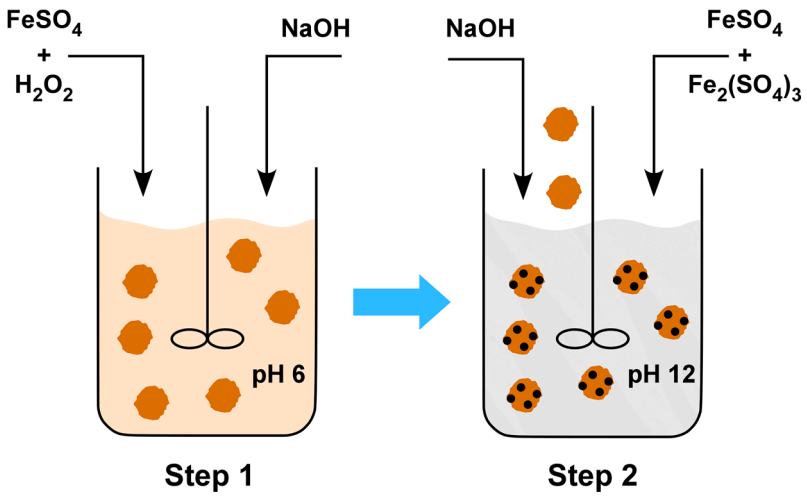

Figure 1. Schematic representation of Fe_3O_4/FeOOH nanocomposites synthesis steps.

For the preparation of pure Fe_3O_4 nanoparticles which served as a reference sample, 7.2 g of $FeSO_4 \cdot 7H_2O$ and 10.8 g of $Fe_2(SO_4)_3 \cdot xH_2O$ were dissolved in 200 mL of distilled water and then the pH was adjusted to 12 by the addition of NaOH solution.

2.2. Characterization

Structural-phase identification was performed by powder X-ray diffractometry (XRD) using a water-cooled Rigaku Ultima+ diffractometer with CuKa radiation, a step size of 0.05° and a step time of 3 s, operating at 40 kV and 30 mA. Scanning electron microscopy (SEM) images were obtained using a Quanta 200 ESEM FEG FEI microscope with a field-emission gun operating at 30 kV. Thermogravimetric analyses (TG-DTA) of the samples were determined with a water-cooled Perkin-Elmer STA 6000 instrument in the temperature range 50–900 °C, at a heating rate of 20 °C/min in nitrogen atmosphere. As an indicator of the reducing potential of the nanocomposite, the ratio of Fe^{2+}/Fe^{3+} was determined by titration. A sample quantity of 0.1 g was dissolved under heating in 50 mL 7 M H_2SO_4 and titrated with 0.05 M $KMnO_4$. The end point of the titration was defined by the persisting weak pink color, indicating that the MnO_4^- ions were no longer being reduced.

2.3. Antimony Adsorption

The efficiency of developed Fe_3O_4/FeOOH nanocomposites to operate as antimony adsorbents was evaluated by adsorption experiments carried out at pH 7 and residual concentrations in the range 0–700 μg/L. Stock solutions of Sb(III) or Sb(V) (100 mg/L) were prepared from Sb_2O_3 and $K[Sb(OH)_6]$, respectively. Then, the working standards were freshly prepared by proper dilution of the stock solutions in a natural-like water prepared according to the National Sanitation Foundation (NSF) standard. To prepare 1 L of natural-like water, 252 mg $NaHCO_3$, 12.14 mg $NaNO_3$, 0.178 mg $NaH_2PO_4 \cdot H_2O$, 2.21 mg NaF, 70.6 mg $NaSiO_3 \cdot 5H_2O$, 147 mg $CaCl_2 \cdot 2H_2O$ and 128.3 mg $MgSO_4 \cdot 7H_2O$ were diluted in distilled water. For the adsorption experiments, a quantity of 5–100 mg of fine powder was placed in 300 mL conical flasks and dispersed in 200 mL of aqueous Sb(III) or Sb(V) solutions. Initial antimony concentrations ranged between 100 and 2000 μg/L. The pH was controlled at 7 throughout the experiment by adding either NaOH or HCl of 0.1 or 0.01 M. The mixture was shaken for 24 h at 20 °C, and then the solid was separated by 0.45 μm pore-size membrane filters. Initial and residual antimony concentrations were determined by graphite furnace atomic absorption spectrophotometry, using a Perkin-Elmer AAnalyst 800 instrument. It should be noted that the adsorption capacity corresponding to a residual Sb(III) or Sb(V) concentration equal to the drinking water regulation limit of 5 μg/L (Q_5-index) was used as an evaluation criterion between samples.

The points obtained by adsorption experiments were fitted by proper functions describing the observed trend. In most cases, a Freundlich-type equation was applied:

$$Q_e = K_F C_e^{1/n}, \quad (1)$$

where Q_e is the amount of Sb adsorbed per mass of adsorbent, C_e the equilibrium concentration, and K_F and n constants relate to adsorption capacity and affinity, respectively. For low-affinity adsorption curves, the isotherms were fitted by the BET (Brunauer, Emmett and Teller) equation for liquid-phase adsorption:

$$Q_e = aC_e/(1 + bC_e + cC_e^2), \quad (2)$$

where a, b and c are constants related to the equilibrium constants for adsorption in the first layer and the upper layers [22].

3. Results

3.1. Material Characterization

The preservation of the participating phases in the formed nanocomposites was verified by structural characterization. Figure 2 presents the XRD diagrams of the Fe_3O_4/FeOOH samples with a gradually increasing percentage of Fe_3O_4, that is, 25, 50 and 75 wt % in comparison to the separately produced pure FeOOH and Fe_3O_4 samples. The iron oxy-hydroxide prepared at pH 6 was stabilized as a low-crystalline iron oxy-hydroxide and identified by the crystal symmetry of ferrihydrite ($Fe_5O_7(OH) \cdot 4H_2O$). The mean crystal size of pure FeOOH was estimated through the broadening of diffraction peaks to be around 5 nm by the application of Scherrer's equation. On the contrary, the introduction of a more crystalline phase such as Fe_3O_4, even at low percentages, resulted in the domination of its intense peaks in the obtained diagrams. The corresponding mean crystal size of Fe_3O_4, as calculated by the XRD diagram of the pure phase, approached 13 nm.

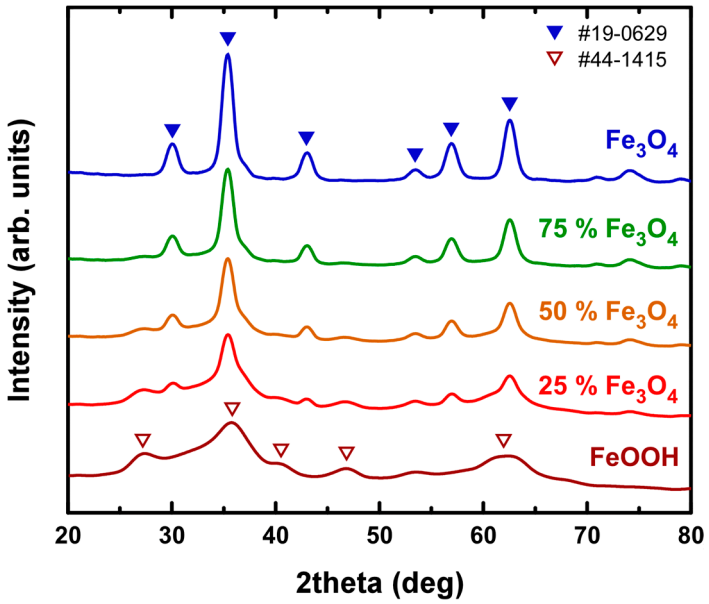

Figure 2. X-ray diffraction diagrams of studied Fe_3O_4/FeOOH nanocomposites. Triangles indicate the expected diffraction angles for magnetite and ferrihydrite from the ICDD/JCPDS PDF Database [23].

The percentage of structural hydroxyls is another indirect parameter to evaluate sample composition. In particular, magnetite-rich samples should present a much lower weight loss during TG-DTA analysis. Indeed, Figure 3 shows a total loss of 20 wt % in the mass of pure FeOOH which proportionally decreased with the gain of Fe_3O_4 percentage. Around 17 wt % of it corresponds to the removal of adsorbed water and the dehydroxylation process occurring in the range 100–300 °C, which is attached to a broad endotherm peak in the DTA curve. The presence of Fe_3O_4 initiates a weak increase of the mass at 200 °C which can be attributed to the adsorption of oxygen traces still existing in the nitrogen flow. Such an effect splits the dehydroxylation in a second endothermic step around 300 °C. The exothermic peak in the range 550–620 °C for all samples is indicative of maghemite transformation to hematite. Finally, the drop of mass in the FeOOH-rich samples above 630 °C is explained by the release of crystallized water molecules originating from the initial ferrihydrite structure.

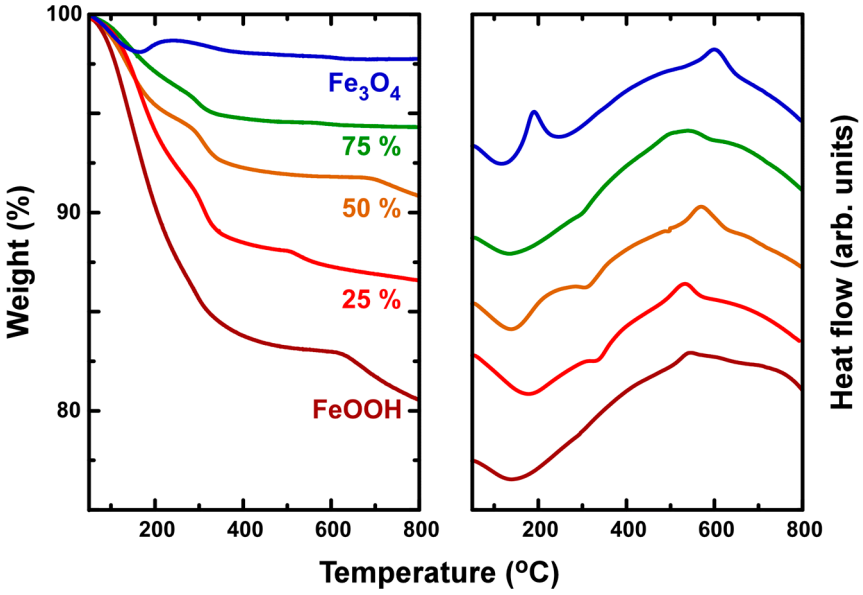

Figure 3. Thermogravimetric and differential thermal analysis for studied Fe_3O_4/FeOOH nanocomposites.

The morphology of the combined phases has been examined through SEM observations (Figure 4). The separate preparation of single-phase Fe_3O_4 by chemical co-precipitation under alkaline conditions is known to result in spherical nanoparticles sized around 40 nm [24]. The image of Figure 4a verifies the small dimensions of building units in the sample. On the contrary, pure FeOOH consists of large grains with high surface roughness and high porosity (Figure 4b) in agreement with the low dimension crystallinity shown in the X-ray spectra. The sequential formation of the two phases contributes to the production of a nanocomposite where Fe_3O_4 nanoparticles are distributed on the surface of the FeOOH grains (Figure 4c).

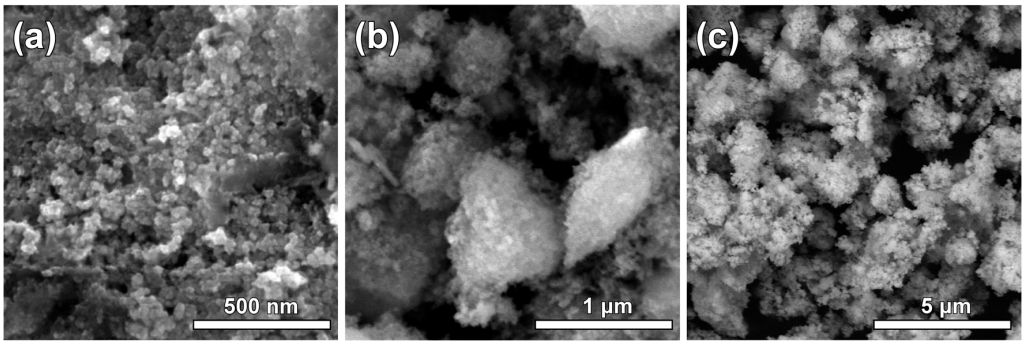

Figure 4. SEM images of (**a**) single-phase Fe_3O_4 sample; (**b**) single-phase FeOOH sample; and (**c**) Fe_3O_4/FeOOH 50 wt % nanocomposite.

3.2. Evaluation of Sb Removal

The efficiency of synthesized Fe_3O_4/FeOOH nanocomposites to capture antimony species was studied by the corresponding adsorption isotherms obtained at low residual concentrations. Figure 5 summarizes the results concerning the removal of Sb(III) at pH 7. In FeOOH-rich samples, isotherms indicate higher capacities where fitting is successful by the Freundlich relation (Equation (1)). However, when the Fe_3O_4 percentage eclipses 50 wt %, the obtained isotherm pattern is significantly modified, suggesting a low-affinity adsorption which is better expressed by the BET equation (Equation (2)). The adsorption capacity of pure FeOOH at a residual concentration of 5 μg/L is found around 2.8 mg/g but rapidly falls as higher quantities of Fe_3O_4 nanoparticles are added to reach 0.27 mg/g for pure magnetite.

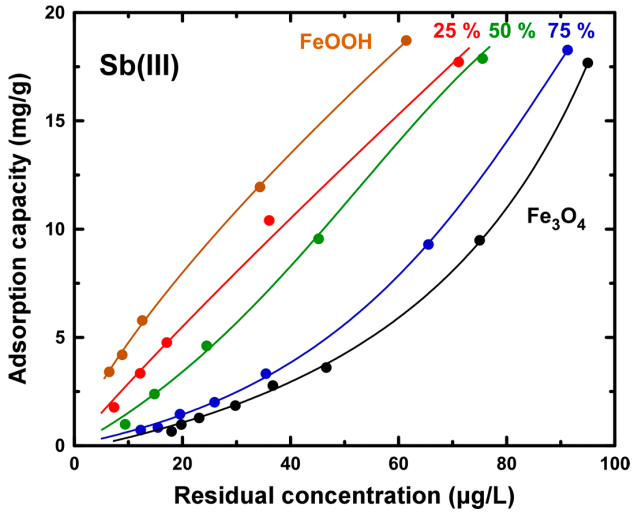

Figure 5. Adsorption isotherms of studied Fe_3O_4/FeOOH nanocomposites for Sb(III) taken in natural-like water adjusted to pH 7. Curves correspond to the fitting by Freundlich or BET equations.

In spite of its negative role in Sb(III) uptake, the incorporation of Fe_3O_4 nanoparticles clearly promotes Sb(V) adsorption which is actually the milestone of this study. The importance of Fe_3O_4 presence is signified by the shift of isotherms from the zero values, at the range of drinking water regulation limit for pure FeOOH, to significant adsorption capacities (Figure 6). Particularly, the estimated Q_5-value gradually increases from 0.29 up to 0.45 mg/g almost proportionally to the Fe_3O_4 percentage. All isotherms follow a Freundlich-type trend concluding a high affinity for adsorption.

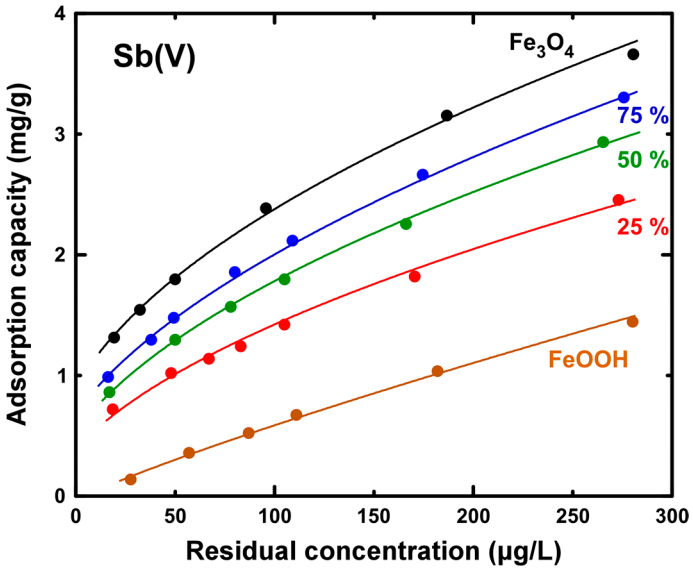

Figure 6. Adsorption isotherms of studied Fe_3O_4/FeOOH nanocomposites for Sb(V) taken in natural-like water adjusted at pH 7. Curves correspond to the Freundlich-type fitting.

Table 1 summarizes the calculated parameters of fitting, either performed by a Freundlich or a BET equation, for the presented Sb(III) and Sb(V) adsorption isotherms.

Table 1. Fitting parameters of adsorption isotherms.

Species	Fe_3O_4 (wt %)	Q_5 (mg/g)	Freundlich		BET		
			K_F	1/n	a	b	c (10^{-5})
Sb(III)	0	2.8	0.825	0.758			
	25	1.5	0.354	0.917			
	50	0.72			0.136	−0.011	7.5
	75	0.28			0.053	−0.013	6.0
	100	0.27			0.051	−0.009	1.6
Sb(V)	0	0.05	0.012	0.840			
	25	0.29	0.123	0.530			
	50	0.38	0.164	0.517			
	75	0.40	0.177	0.510			
	100	0.45	0.202	0.505			

4. Discussion

The addition of a reducing phase such as Fe_3O_4 in typical water adsorbents like iron oxy-hydroxides indicated an improvement in the uptake of Sb(V) species with respect to the realization of residual concentrations below 5 μg/L. An overview of the enhancing trend in correlation to the percentage of Fe_3O_4 nanoparticles in the nanocomposite is shown in Figure 7. In addition, the improvement of adsorption capacity and affinity at higher Fe_3O_4 percentages is also reflected in the increase of K_F and decrease of 1/n (Table 1). Considering that even freshly prepared ferric

hydroxides cannot bring Sb(V) removal capacities above 0.1 mg/g for equilibrium concentrations of 10 μg/L [25], the Q_5-values of at least 0.3 mg/g support the important contribution of Fe_3O_4 in efficiency improvement. The ability of Fe_3O_4 to operate as electron donor enables the reduction of Sb(V) to Sb(III) oxy-ions which are then captured by the iron oxy-hydroxide that shows higher affinity to antimonite species. The effect of Fe oxidation state in the adsorption capacity for Sb(V) has been also observed for reduced nontronite [26], whereas the high affinity of ≡FeOH sites for antimony species has been demonstrated in iron-oxide-rich red-earth soils [27]. In a similar approach, the combination of an oxidative manganese compound with an iron oxy-hydroxide adsorbent, in single- [28] or binary-phase [29] materials, was applied as a sophisticated way to oxidize As(III) and then capture it as As(V).

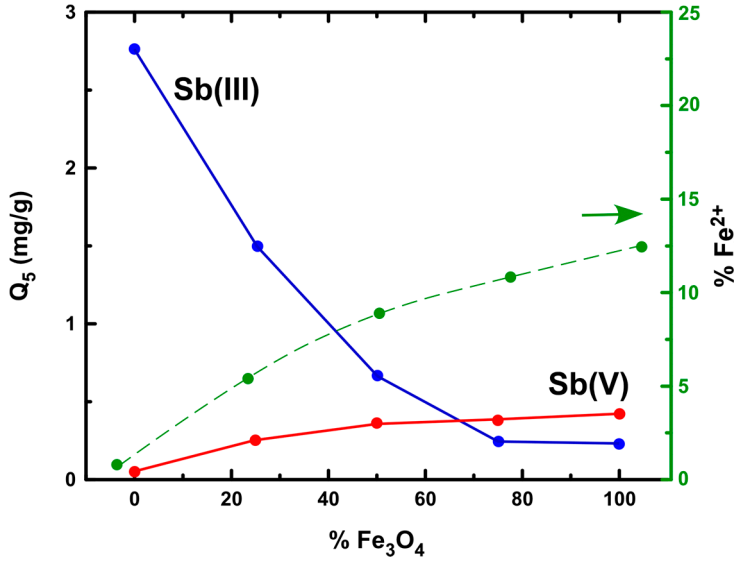

Figure 7. Variation of adsorption capacity for Sb(III) and Sb(V) corresponding to the drinking water regulation limit for the studied Fe_3O_4/FeOOH nanocomposites. The evolution of Fe^{2+} percentage with Fe_3O_4 content is also indicated.

The reducing potential of the nanocomposites increases almost proportionally to the percentage of Fe_3O_4. Titration measurements indicate that Fe^{2+} represents a significant part of the total mass of the nanocomposite, approaching 12.5 wt % in the pure Fe_3O_4 sample. Nevertheless, the improvement degree of Sb(V) uptake capacity at higher Fe_3O_4 and Fe^{2+} percentages does not follow the expectations arising by the significant increase of reducing potential. Such an observation is attributed to the decreasing presence of FeOOH, which is a better adsorbent for Sb(III), and to the increasing number of Fe_3O_4 nanoparticles occupying the surface of the nanocomposite.

At the same time, the adsorption efficiency for Sb(III) shows a dramatic decrease during the rise of Fe_3O_4 percentage in the nanocomposite. At 50 wt % Fe_3O_4, the Q_5-value drops by almost one order of magnitude, becoming even lower than the corresponding capacity for Sb(V). This is consistent with a lower activity of directly adsorbed Sb(III) species in comparison to Sb(III) originating from the reduction of Sb(V). At the same time, the surface oxidation of Fe_3O_4 nanoparticles generates freshly formed adsorption sites where secondarily formed Sb(III) species are chemisorbed with higher efficiency. Therefore, an optimum composition of the nanocomposite is suggested to be around 25 wt % Fe_3O_4 considering that Sb(V) uptake is almost maximized but Sb(III) removal is still preserved at high levels. It should be underlined that the most critical point of this work is to introduce, for the first time, an adsorbent with at least a low adsorption capacity for Sb(V) which, however, fulfills the drinking water regulation limit. Actually, the Sb(V) species are the dominant ones in commonly used water sources. To this end, even a significant efficiency loss for Sb(III) can be affordable as long as it is not related to any effect in the Sb(V) uptake or to the elevation of the nanocomposite's synthesis cost.

5. Conclusions

The combination of an iron oxy-hydroxide showing good affinity for Sb(III) with an iron oxide (Fe_3O_4) known for its reducing potential has been studied as a way to develop an adsorbent oriented to the treatment of antimony-polluted water. In particular, a series of Fe_3O_4/FeOOH nanocomposites with different composition ratios were prepared by sequential chemical precipitation of iron salts. The addition of Fe_3O_4 is the key to initiate the uptake of Sb(V) species through a mechanism of reduction to Sb(III) followed by the chemisorption onto the FeOOH surface. Importantly, the efficiency of these adsorbents is extended to the low residual concentrations range including the drinking water regulation limit for antimony. That sets the application of Fe_3O_4/FeOOH nanocomposites among the first adsorption processes with practical interest in Sb(V) removal. Another aspect of this study, not discussed in this paper, arises by the magnetic response of the nanocomposites due to Fe_3O_4 which enables the possibility for alternative application schemes based on magnetic separation. Furthermore, the suggested approach of reduction–adsorption can be extended in future research on various other materials known for such properties.

Author Contributions: K.S. and M.M. conceived, designed and supervised the experiments. K.K., E.K., G.M. and T.A. performed the synthesis and adsorption experiments. T.A. and L.B. performed materials characterization measurements and evaluation. K.S. wrote the paper with the contribution of all co-authors.

Funding: This scientific work was implemented within the frame of the action "Supporting Postdoctoral Researchers" of the Operational Program "Development of Human Resources, Education and Lifelong Learning 2014–2020" of IKY State Scholarships Foundation and is co-financed by the European Social Fund and the Greek State. Financial support from the Spanish Ministry of Economy and Competitiveness through the "Severo Ochoa" Programme for Centres of Excellence in R&D (SEV-2015-0496), and project MAT2015-71664-R is also acknowledged. SEM measurements received funding from the EU-H2020 research and innovation program under grant agreement No 654360 having benefitted from the access provided by CSIC-ICMAB in Barcelona within the framework of the NFFA-Europe Transnational Access Activity. Authors would like to thank Anna Esther Carrillo for the experimental assistance during SEM observations.

Conflicts of Interest: The authors declare no conflict of interest. The funders had no role in the design of the study; in the collection, analyses, or interpretation of data; in the writing of the manuscript, or in the decision to publish the results.

References

1. Filella, M.; Belzile, N.; Chen, Y.-W. Antimony in the environment: A review focused on natural waters: I. Occurrence. *Earth-Sci. Rev.* **2002**, *57*, 125–176. [CrossRef]
2. Herath, I.; Vithanage, M.; Bundschuh, J. Antimony as a global dilemma: Geochemistry, mobility, fate and transport. *Environ. Pollut.* **2017**, *223*, 545–559. [CrossRef] [PubMed]
3. US Environmental Protection Agency. *Edition of the Drinking Water Standards and Health Advisories*; US Environmental Protection Agency: Washington, DC, USA, 2012.
4. Scheinost, A.C.; Rossberg, A.; Vantelon, D.; Xifra, I.; Kretzschmar, R.; Leuz, A.K.; Funke, H.; Johnson, C.A. Quantitative antimony speciation in shooting-range soils by EXAFS spectroscopy. *Geochim. Cosmochim. Acta* **2006**, *70*, 3299–3312. [CrossRef]
5. Wu, Z.; He, M.; Guo, X.; Zhou, R. Removal of antimony (III) and antimony (V) from drinking water by ferric chloride coagulation: Competing ion effect and the mechanism analysis. *Sep. Purif. Technol.* **2010**, *76*, 184–190. [CrossRef]
6. Li, X.; Dou, X.; Li, J. Antimony(V) removal from water by iron-zirconium bimetal oxide: Performance and mechanism. *J. Environ. Sci.* **2012**, *24*, 1197–1203. [CrossRef]
7. Mitrakas, M.; Mantha, Z.; Tzollas, N.; Stylianou, S.; Katsoyiannis, I.; Zouboulis, A. Removal of Antimony Species, Sb(III)/Sb(V), from Water by Using Iron Coagulants. *Water* **2018**, *10*, 1328.
8. Wu, D.; Sun, S.-P.; He, M.; Wu, Z.; Xiao, J.; Chen, X.D.; Wu, W.D. As(V) and Sb(V) co-adsorption onto ferrihydrite: Synergistic effect of Sb(V) on As(V) under competitive conditions. *Environ. Sci. Pollut. Res.* **2018**, *25*, 14585–14594. [CrossRef] [PubMed]
9. Ungureanu, G.; Santos, S.; Boaventura, R.; Botelho, C. Arsenic and antimony in water and wastewater: Overview of removal techniques with special reference to latest advances in adsorption. *J. Environ. Manag.* **2015**, *151*, 326–342. [CrossRef]

10. Xu, C.; Zhang, B.; Zhu, L.; Lin, S.; Sun, X.; Jiang, Z.; Tratnyek, P.G. Sequestration of antimonite by zerovalent iron: Using weak magnetic field effects to enhance performance and characterize reaction mechanisms. *Environ. Sci. Technol.* **2016**, *50*, 1483–1491. [CrossRef]
11. Leng, Y.; Guo, W.; Su, S.; Yi, C.; Xing, L. Removal of antimony(III) from aqueous solution by graphene as an adsorbent. *Chem. Eng. J.* **2012**, *211–212*, 406–411. [CrossRef]
12. Xu, Y.; Ohki, A. Adsorption and removal of antimony from aqueous solution by an activated alumina. *Toxicol. Environ. Chem.* **2001**, *80*, 145–154. [CrossRef]
13. Wingenfelder, U.; Furrer, G.; Schulin, R. Sorption of antimonate by HDTMA-modified zeolite. *Microporous Mesoporous Mater.* **2006**, *95*, 265–271. [CrossRef]
14. Simeonidis, K.; Papadopoulou, V.; Tresintsi, S.; Kokkinos, E.; Katsoyiannis, I.; Zouboulis, A.; Mitrakas, M. Efficiency of iron-based oxy-hydroxides in removing antimony from groundwater to levels below the drinking water regulation limits. *Sustainability* **2017**, *9*, 238. [CrossRef]
15. Shan, C.; Ma, Z.; Tong, M. Efficient removal of trace antimony(III) through adsorption by hematite modified magnetic nanoparticles. *J. Hazard. Mater.* **2014**, *268*, 229–236. [CrossRef]
16. Ilavský, J.; Barloková, D.; Hudec, P.; Munka, K. Iron-based sorption materials for the removal of antimony from water. *J. Water Supply Res. Technol.* **2014**, *63*, 518–524. [CrossRef]
17. Miao, Y.; Han, F.; Pan, B.; Niu, Y.; Nie, G.; Lv, L. Antimony(V) removal from water by hydrated ferric oxides supported by calcite sand and polymeric anion exchanger. *J. Environ. Sci.* **2014**, *26*, 307–314. [CrossRef]
18. Mishra, S.; Dwivedi, J.; Kumar, A.; Sankararamakrishnan, N. Removal of antimonite (Sb(III)) and antimonate (Sb(V)) using zerovalent iron decorated functionalized carbon nanotubes. *RSC Adv.* **2016**, *6*, 95865–95878. [CrossRef]
19. Belzile, N.; Chen, Y.W.; Wang, Z. Oxidation of antimony (III) by amorphous iron and Manganese oxyhydroxides. *Chem. Geol.* **2001**, *174*, 379–387. [CrossRef]
20. Qi, P.; Pichler, T. Sequential and simultaneous adsorption of Sb(III) and Sb(V) on ferrihydrite: Implications for oxidation and competition. *Chemosphere* **2016**, *145*, 55–60. [CrossRef]
21. Tresintsi, S.; Simeonidis, K.; Zouboulis, A.; Mitrakas, M. Comparative study of As(V) removal by ferric coagulation and oxy-hydroxides adsorption: Laboratory and full-scale case studies. *Desalin. Water Treat.* **2013**, *51*, 2872–2880. [CrossRef]
22. Ebadi, A.; Soltan Mohammadzadeh, J.S.; Khudiev, A. What is the correct form of BET isotherm for modeling liquid phase adsorption? *Adsorption* **2009**, *15*, 65–73. [CrossRef]
23. *Powder Diffraction File*, 2004th ed.; Joint Center for Powder Diffraction Studies, International Centre for Diffraction Data: Newtown Square, PA, USA, 2004.
24. Simeonidis, K.; Kaprara, E.; Samaras, T.; Angelakeris, M.; Pliatsikas, N.; Vourlias, G.; Mitrakas, M.; Andritsos, N. Optimizing magnetic nanoparticles for drinking water technology: The case of Cr(VI). *Sci. Total Environ.* **2015**, *535*, 61–68. [CrossRef] [PubMed]
25. He, Z.; Liu, R.; Liu, H.; Qu, J. Adsorption of Sb(III) and Sb(V) on freshly prepared ferric hydroxide (FeO_xH_y). *Environ. Eng. Sci.* **2015**, *32*, 95–102. [CrossRef] [PubMed]
26. Ilgen, A.G.; Trainor, T.P. Sb(III) and Sb(V) sorption onto Al-rich phases: Hydrous Al oxide and the clay minerals kaolinite KGa-1b and oxidized and reduced nontronite NAu-1. *Environ. Sci. Technol.* **2012**, *46*, 843–851. [CrossRef] [PubMed]
27. Vithanage, M.; Rajapaksha, A.U.; Dou, X.; Bolan, N.S.; Yang, J.E.; Ok, Y.S. Surface complexation modeling and spectroscopic evidence of antimony adsorption on iron-oxide-rich red earth soils. *J. Colloid Interface Sci.* **2013**, *406*, 217–224. [CrossRef] [PubMed]

28. Tresintsi, S.; Simeonidis, K.; Estradé, S.; Martinez-Boubeta, C.; Vourlias, G.; Pinakidou, F.; Katsikini, M.; Paloura, E.C.; Stavropoulos, G.; Mitrakas, M. Tetravalent manganese feroxyhyte: A novel nanoadsorbent equally selective for As(III) and As(V) removal from drinking water. *Environ. Sci. Technol.* **2013**, *47*, 9699–9705. [CrossRef] [PubMed]
29. Zhang, G.; Liu, F.; Liu, H.; Qu, J.; Liu, R. Respective role of Fe and Mn oxide contents for arsenic sorption in iron and manganese binary oxide: An X-ray absorption spectroscopy investigation. *Environ. Sci. Technol.* **2014**, *48*, 10316–10322. [CrossRef]